Dendritic PARACEST contrast agents for magnetic resonance imaging

CONTRAST MEDIA & MOLECULAR IMAGING
Contrast Media Mol. Imaging **2**:229–239 (2007)
Published online 16 October 2007 in Wiley InterScience (www.interscience.wiley.com) DOI:10.1002/cmmi.149

CONTRAST MEDIA & MOLECULAR IMAGING

Full Paper

Dendritic PARACEST contrast agents for magnetic resonance imaging

J.A. Pikkemaat[1], R.T. Wegh[1], R. Lamerichs[1], R.A. van de Molengraaf[1], S. Langereis[1], D. Burdinski[1], A.Y.F. Raymond[1,2], H.M. Janssen[3], B.F.M. de Waal[2], N.P. Willard[1], E.W. Meijer[2] and H. Grüll[1]*

[1]*Philips Research Europe, High Tech Campus 11, 5656 AE Eindhoven, The Netherlands*
[2]*Eindhoven University of Technology, Laboratory of Macromolecular and Organic Chemistry, PO Box 513, 5600 MB Eindhoven, The Netherlands*
[3]*SyMO-Chem BV, PO Box 513, 5600 MB Eindhoven, The Netherlands*

Received 8 June 2007; Revised 17 August 2007; Accepted 23 August 2007

ABSTRACT: MRI contrast agents based on chemical exchange-dependent saturation transfer (CEST), such as Yb(III)-DOTAM complexes, are highly suitable for pH mapping. In this paper, the synthesis of Yb(III)DOTAM-functionalized poly(propylene imine) dendrimers is described. The applicability of these dendritic PARACEST MRI agents for pH mapping has been evaluated on a 7 T NMR spectrometer and on a 3 T clinical MRI scanner. As expected, based on the different numbers of exchangeable amide protons, the lowest detectable concentration of the first and third generation dendritic PARACEST agents is by a respective factor of about 4 and 16 lower than that of a mononuclear reference complex. The pH dependence of the CEST effect observed for these compounds depends on the generation of the poly(propylene imine) dendrimer. Upon going to higher generations of the Yb(III)DOTAM-terminated dendrimer, a shift of the maximum CEST effect towards lower pH values was observed. This allows for a fine-tuning of the responsive pH region by varying the dendritic framework. Copyright © 2007 John Wiley & Sons, Ltd.

KEYWORDS: magnetic resonance imaging (MRI); PARACEST contrast agents; ytterbium; DOTAM; poly(propylene imine) dendrimers; pH mapping; molecular imaging

INTRODUCTION

Chemical exchange-dependent saturation transfer (CEST) is a novel technique for MRI contrast enhancement. It relies on altering the water signal intensity by selectively saturating the resonance frequency of exchangeable hydrogen atoms of a CEST contrast agent (CA). CEST as well as Gd(III)-based MRI CAs are highly suited as pH reporters (1–8). pH mapping with MRI is of great clinical importance, since the pH in tumorous and infarcted tissue is different from that in healthy tissue (9). In contrast to conventional T_1-based CAs, CEST MRI probes also allow for multiplexing by using a compound or a mixture of compounds with different exchangeable-proton resonances, which is of particular interest for molecular imaging (10). Moreover, the CEST MRI contrast enhancement can be turned on and off by means of a selective radiofrequency pulse needed for saturation of the exchangeable-proton signal. Adjustable contrast enhancement is highly advantageous for applications with a slow uptake of the CA, such as molecular imaging(11) or lymph-node staging (12–14). The CEST MRI reference image can be recorded immediately before or after the contrast-enhanced image. Hence, a single MRI examination is sufficient and the spatial alignment of the reference and contrast-enhanced images is improved.

The magnitude of the saturation transfer, the CEST effect, ST%, is usually calculated according to eqn (1) (15).

$$\mathrm{ST}\% = (1 - M_S/M_0) \cdot 100\% \qquad (1)$$

Here, M_S is the intensity of an MR image taken immediately after an RF saturation pulse has been applied at the resonance frequency of the CA's exchangeable protons. M_0 is the intensity of the reference image, which is recorded after the RF saturation pulse has been applied symmetrically on the opposite side of the bulk water signal to correct for non-selective saturation, most prominently direct water saturation. Using rapid imaging techniques or interleaved acquisition of both images, the time interval between recording the 'pre-saturated' and the reference image is only slightly longer than the time needed for the application of the saturation pulse, typically a few seconds.

**Correspondence to*: J.A. Pikkemaat, Department of Materials Analysis, Philips Research Europe, High Tech Campus 11 (PO Box 01), 5656 AE Eindhoven, The Netherlands.
E-mail: jeroen.pikkemaat@philips.com
Contract/grant sponsor: Dutch BSIK-Program Molecular Imaging of Ischemic Heart Disease; *contract/grant number:* BSIK03033.

A major clinical limitation for CEST imaging is its relatively low sensitivity. First-generation CEST CAs showed an estimated detection limit (ST% = 5%) of 20 mM (at 7 T), which is too high for clinical applications for reasons of toxicity (16). In theory, there are several ways to improve this sensitivity.

One strategy is based on enhancing the exchange rate of the protons. In a two-site exchange model, at complete saturation of the exchangeable proton resonance, and in the absence of direct saturation of the bulk water resonance and background magnetization transfer, M_S/M_0 is given by eqn (2) (17,18).

$$M_S/M_0 = 1/(1 + k_{obs}T_{1sat}) \quad (2a)$$

$$k_{obs} = n[CA]/2[H_2O]\tau_M \quad (2b)$$

T_{1sat} is the spin-lattice relaxation time of the bulk water protons during saturation of the exchanging protons and k_{obs} is the pseudo-first-order exchange rate constant, where [CA] is the concentration of the CEST CA, n is the number and τ_M is the life-time of the exchangeable protons. In the case of exchangeable amide protons, τ_M depends on the pH. This implies that CEST MRI CAs can be used for pH mapping (19). The CEST effect could, therefore, be increased by reducing τ_M. Concomitantly, in order to avoid coalescence of the exchangeable proton with the bulk water signal, the chemical-shift difference between the exchangeable-proton resonance and the water resonance ($\Delta\omega$) should be increased ($\tau_M\Delta\omega > 1$) (19). Large chemical-shift differences (up to several hundreds of ppm) are known for protons in the proximity of a paramagnetic lanthanide ion. Initial studies of this type of CEST agents, called PARACEST agents, were conducted using lanthanide-chelates of either DOTAM(20) or DOTAM-Gly (21). As a result of the large chemical-shift difference between water and the exchangeable amide hydrogen atoms (about −16 ppm for the Yb(III) complexes), these systems are the most sensitive PARACEST agents reported so far, with an experimental detection limit of approximately 0.5 mM at 7 T. In different types of PARACEST agents the resonance frequency of slowly exchanging lanthanide-bound water molecules is saturated to obtain a CEST effect (21–23). In theory, a detection limit in the order of 0.01 mM should be feasible for PARACEST agents with a τ_M of 3 μs and a $\Delta\omega$ of 500 ppm (23). This detection limit is of the same order or even lower than those typically observed for low molecular weight T_1-based MRI CAs (24).

A second strategy to improve the sensitivity of CEST is based on polymeric agents with a large number of exchangeable groups per polymer molecule that can be saturated simultaneously. Initial studies on polymeric CEST agents were reported by Goffeney *et al.*(25). In their work, CEST effects of approximately 40% were achieved using a 0.1 mM solution of poly-L-lysine, containing per molecule about 2300 exchangeable backbone amide protons. The CEST frequencies of diamagnetic agents, however, lie inherently close to the resonance frequencies of endogenous compounds. Special precautions are therefore needed to suppress artefacts that arise *in vivo* from the asymmetry in the conventional magnetization transfer contrast and those caused by direct saturation (26,27).

The lowest detection limits are expected for macromolecular PARACEST agents with a large number of chemically equivalent, exchangeable amide protons. Thus far, only two such CEST agents have been described in the literature, one based on supramolecular adducts between poly-L-arginine and Tm(III)DOTP(28) and a second based on DOTAM-like conjugates with poly-L-lysine (29). An alternative approach to obtain highly sensitive CEST agents based on liposomes has recently been introduced by Aime *et al* (30,31).

In this study, we have investigated new CEST MRI agents based on dendrimers for pH mapping. These well-defined, highly branched macromolecules, with a tunable size and nanoscopic dimensions, had already been employed successfully as multivalent T_1-based MRI CAs (32–36). It had been demonstrated that the pharmacokinetic properties of dendritic CAs strongly depend on the size, i.e. the generation of the dendrimer, and the nature of the dendritic scaffold. For instance, higher generations of Gd(III)DTPA-terminated poly(propylene imine) dendrimers, in contrast to low-molecular-weight MRI CAs, remain in the blood in a higher concentration for prolonged periods of time (35). As a result vascular structures are visualized more easily. Another unique feature of poly(propylene imine) dendrimers is that the local pH can be modulated by the tertiary amines of the dendritic core, which is of particular interest for pH-responsive CAs (37). Owing to the symmetrical nature of dendrimers, all Yb(III)DOTAM groups of our dendritic CEST agent were expected to be equivalent, resulting in a lower CEST detection limit. In the present study, different generations of poly(propylene imine) dendrimers were functionalized with Yb(III)DOTAM complexes (Fig. 1) and the applicability of these dendritic structures as pH-responsive PARACEST agents has been studied.

RESULTS AND DISCUSSION

Synthesis

To enable the coupling of Yb(III)DOTAM complexes to different generations of amine-terminated poly(propylene imine) dendrimers, a novel synthetic strategy to obtain DOTAM-based building block **7** has been developed (Fig. 2).

The reaction of **7** with the primary amines of the first and third generations of the poly(propylene imine) dendrimer (with, respectively, 4 and 16 end groups) was performed in DMF with 2-(1*H*-benzotriazole-1-yl)-1,1,3,3-tetramethyluronium hexafluorophosphate (HBTU) and

DOI: 10.1002/cmmi

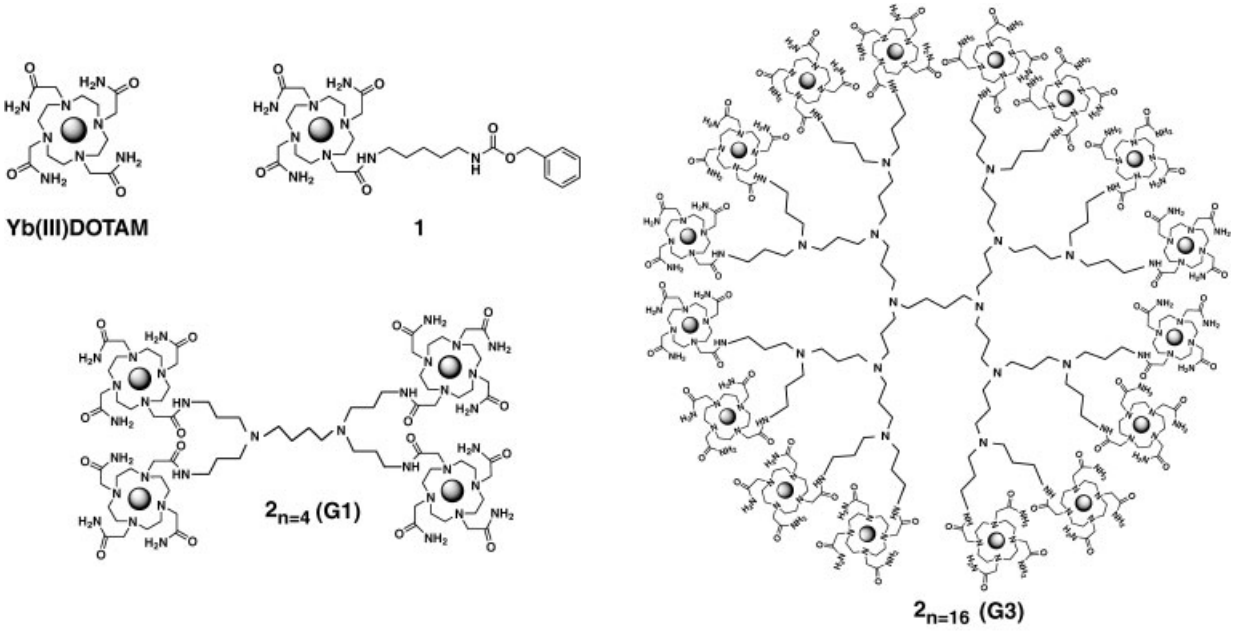

Figure 1. Schematic representation of Yb(III)DOTAM, complex **1**, and different generations of the Yb(III)DOTAM-terminated poly(propylene imine) dendrimers ($\mathbf{2}_n$). G represents the generation of the dendrimer and *n* denotes the theoretical number of Yb(III)DOTAM complexes per dendrimer. The gray balls represent Yb^{3+} ions. Coordinative bonds and the coordinated water molecules have been omitted for clarity.

N,*N*-diisopropylethylamine (DiPEA; Fig. 3). Structural characterization of the DOTAM-terminated dendrimers with MALDI-TOF-MS, ^{1}H NMR and ^{13}C NMR showed complete modification of the primary amines of the poly (propylene imine) dendrimers. After dialysis and lyophilization, the DOTAM-terminated dendrimers ($\mathbf{8}_{n=4,16}$) were allowed to react with $YbCl_3$ to yield dendritic PARACEST agents ($\mathbf{2}_{n=4,16}$).

The synthesis of complex **1**, starting from **7**, was similar to the preparation of the dendritic PARACEST CAs, except that mono *N*-Cbz-protected-1,5-pentamethylenediamine was used as the starting material (Fig. 4).

^{1}H NMR spectroscopy

The one-dimensional ^{1}H NMR spectrum of Yb(III)DOTAM is depicted in Fig. 5(a). Yb(III)DOTAM has a strong predominance of a capped square antiprismatic

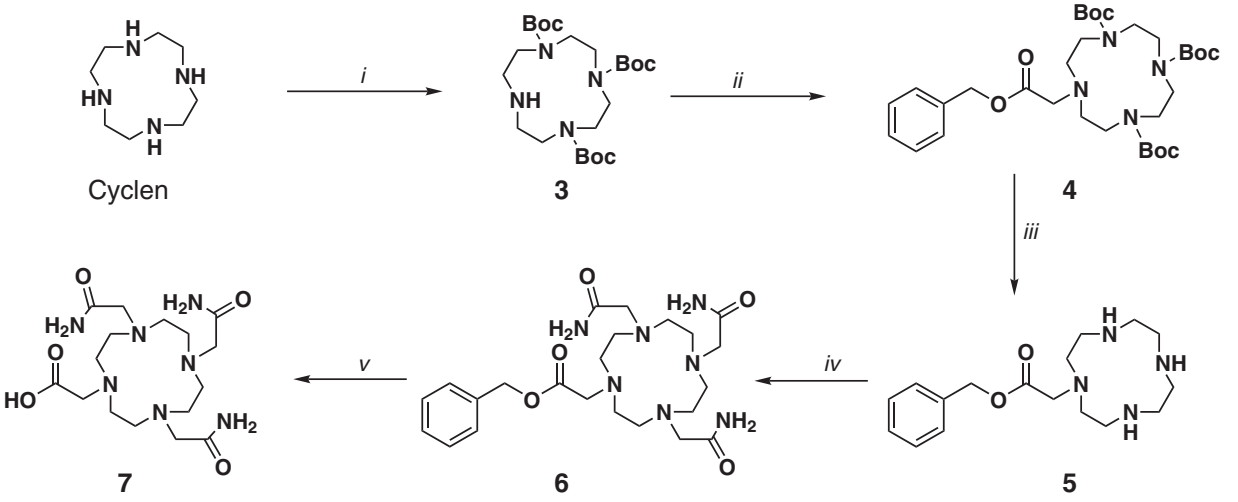

Figure 2. Synthesis of DOTAM-based building block (**7**). (i) Di-tert-butyl dicarbonate, $CHCl_3$,(50) (ii) benzylbromoacetate, DiPEA, CH_3CN, (iii) TFA, DCM, (iv) 2-bromoacetamide, DiPEA, DMF and (v) H_2(g), Pd/C, H_2O.

DOI: 10.1002/cmmi

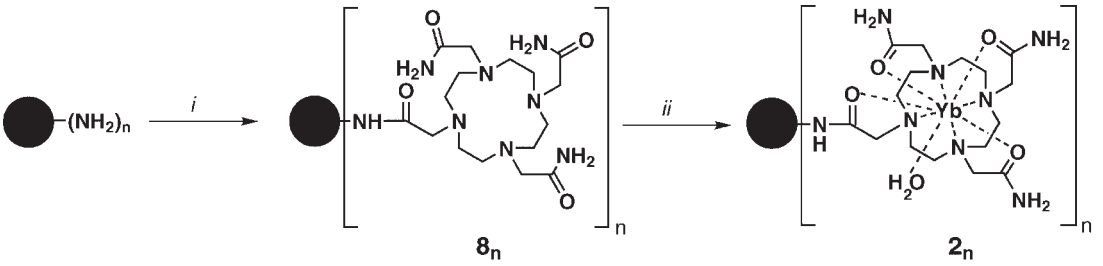

Figure 3. Synthesis of Yb(III)DOTAM-terminated poly(propylene imine) dendrimers ($\mathbf{2}_{n=4,16}$). (i) **7**, DiPEA, HBTU, DMF and (ii) $YbCl_3 \cdot 6H_2O$, H_2O.

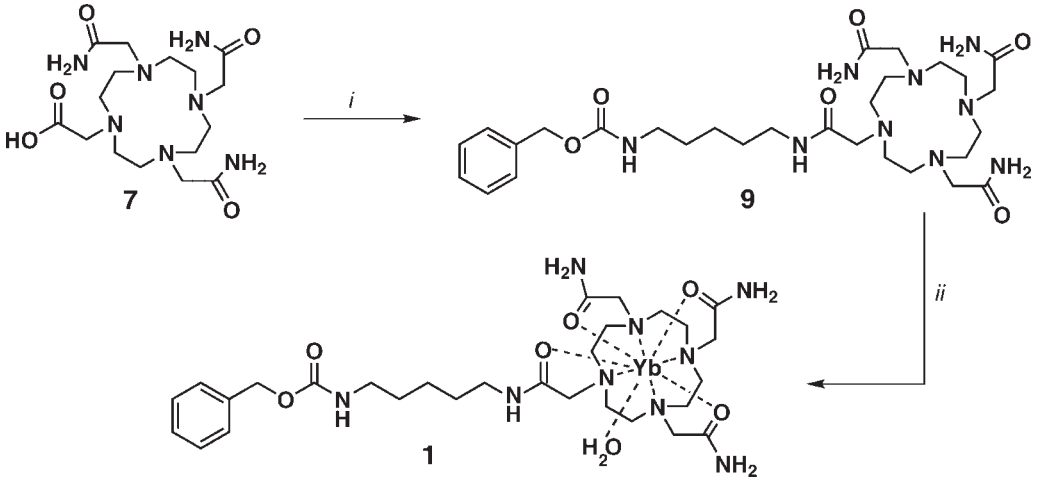

Figure 4. Synthesis of complex **1**. (i) (5-Aminopentyl)carbamic acid benzyl ester, HBTU, DiPEA, DMF, and (ii) $YbCl_3 \cdot 6H_2O$, H_2O.

coordination geometry. The assignment of the respective ^1H and ^{13}C NMR resonances was reported previously (20,21). The one-dimensional ^1H NMR spectra of complex **1** and the different generations of Yb(III)DOTAM-terminated dendrimers ($\mathbf{2}_{n=4,16}$), depicted in Fig. 5b–d, respectively, show signals at similar chemical shifts to Yb(III)DOTAM, suggesting a similar coordination geometry. As can be seen, for example, for the axial CH_2 protons of the cyclen ring at 95 ppm, the C_4 symmetry of Yb(III)DOTAM is disturbed in complex **1** and in the Yb(III)DOTAM-terminated poly(propylene imine) dendrimers ($\mathbf{2}_{n=4,16}$), due to the substitution of one of the amide protons. All signals that originate from the groups of four magnetically equivalent protons of the unsubstituted Yb(III)DOTAM are split up in four distinguishable signals.

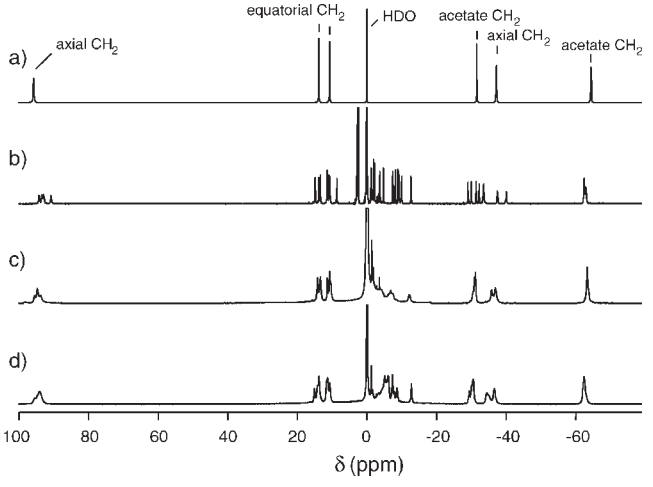

Figure 5. ^1H NMR spectra of (a) Yb(III)DOTAM, (b) complex **1**, (c) $\mathbf{2}_{n=4}$ (G1) and (d) $\mathbf{2}_{n=16}$ (G3) in D_2O at 7 T and RT. The chemical shift of HDO was set at 0 ppm.

In the ^1H NMR spectrum of complex **1**, 10 separate non-exchangeable proton signals are present in the region between −1 and −12 ppm (relative to the water signal), which are all interconnected through J couplings, as observed in the two-dimensional TOCSY spectrum (see supplementary information Figures S1 and S2). These signals are attributed to the 10 protons of the pentamethylene moiety of the molecule. Finally, four non-exchangeable proton signals were found at 0.31, 2.42, 2.75 and 2.95 ppm (relative to the water signal), which all show mutual cross peaks in the TOCSY spectrum. These signals are attributed to the benzyl group

DOI: 10.1002/cmmi

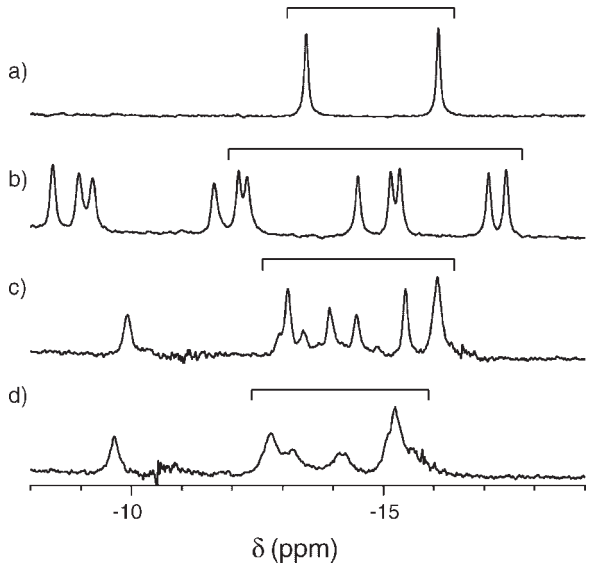

Figure 6. Part of the ^{1}H NMR spectra of (a) Yb(III)DOTAM, (b) complex **1**, (c) $\mathbf{2}_{n=4}$ (G1) and (d) $\mathbf{2}_{n=16}$ (G3) in H_2O at 7 T, 310 K and pH 3.4, showing the exchangeable amide-proton signals (indicated by the bars). The signals around −10 ppm originate from non-exchangeable protons of the linking group. The chemical shift of H_2O was set at 0 ppm.

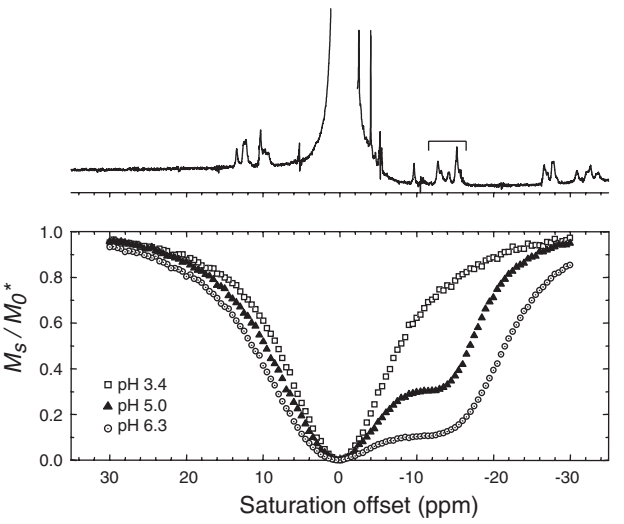

Figure 7. *Z* spectra of an aqueous solution (6 mM MOPS) of the third-generation dendritic PARACEST agent $\mathbf{2}_{n=16}$ [$c(\mathbf{2}_{n=16}) = 1.9$ mM; $c(\text{Yb}) = 30$ mM] at three different pH values at 7 T and 310 K. The amide protons are indicated by the bar. *Z* spectra were recorded using continuous-wave irradiation (2 s duration; 22 μT amplitude) for selective pre-saturation at 150 Hz intervals centered around the water frequency.

of complex **1**. The ^{1}H NMR spectra of the first and third generation Yb(III)DOTAM-terminated poly(propylene imine) dendrimers ($\mathbf{2}_{n=4,16}$) show signals at similar chemical shifts to those of complex **1**, except for the signals of the benzylic protons, which are not present in the dendritic structures. The ^{1}H NMR line widths of the dendritic molecules ($\mathbf{2}_{n=4,16}$) are significantly larger than those of **1**, as a result of the higher molecular weight. Figure 6 shows the ^{1}H NMR spectral region around −15 ppm of Yb(III)DOTAM, complex **1** and the dendritic PARACEST agents ($\mathbf{2}_{n=4,16}$) in H_2O at pH 3.4. For Yb(III)DOTAM (Fig. 6a), two resonances were found, each representing four amide protons (−13.5 and −16.1 ppm relative to the water signal). For complex **1** (Fig. 6b), seven signals were observed that were not present in D_2O. These signals are attributed to the seven exchangeable amide protons of the substituted DOTAM moiety and have similar chemical shifts (−12.2, −12.4, −14.4, −15.2, −15.4, −17.1 and −17.4 ppm relative to the water signal) to the two amide signals of Yb(III)-DOTAM. In the case of the Yb(III)DOTAM-terminated poly(propylene imine) dendrimers, the amide signals are clearly present in the same chemical shift region (Fig. 6c,d). The seven expected signals are not completely resolved.

CEST spectra at 7 T

CEST spectra were recorded of all PARACEST agents as a function of pH. Figure 7 shows CEST spectra of the third-generation dendritic PARACEST agent $\mathbf{2}_{n=16}$ at different pH values. At pH 3.4, the amide protons around −15 ppm presumably exchange too slowly to obtain a reasonable CEST effect. $M_S/M_0{}^*$ decreases upon going from 30 towards 0 ppm, which is due to direct bulk water saturation and is therefore symmetrical around 0 ppm. At higher pH an additional, asymmetrical water signal decrease occurs at the offset frequency of the amide protons. This relative decrease represents the CEST effect due to selective saturation and subsequent exchange of the amide protons.

CEST vs pH

To evaluate the suitability of the PARACEST agents as pH-responsive MRI CAs, the CEST effect of **1** and the Yb(III)DOTAM-terminated dendrimers was measured as a function of the pH at 310 K and at 7 T (Fig. 8). The CEST effect of **1** showed the same pH dependence as that of Yb(III)DOTAM, which was previously reported by Zhang *et al* (20). From pH 5 to 7 a steep increase of the CEST effect was observed, presumably due to a strong increase of the amide proton exchange rate. The amide-proton exchange is both acid- and base-catalyzed, with the base-catalyzed pathway being more effective by several orders of magnitude, for example, in the case of uncoordinated peptides (38). Coordination of a metal ion, such as Yb^{3+}, to the amide oxygen imposes a positive charge on the amide group, which repels nearby protons and increases the acidity of the amide hydrogen atoms (39–41). This is expected to further facilitate the base- over the acid-catalyzed proton exchange pathway.

DOI: 10.1002/cmmi

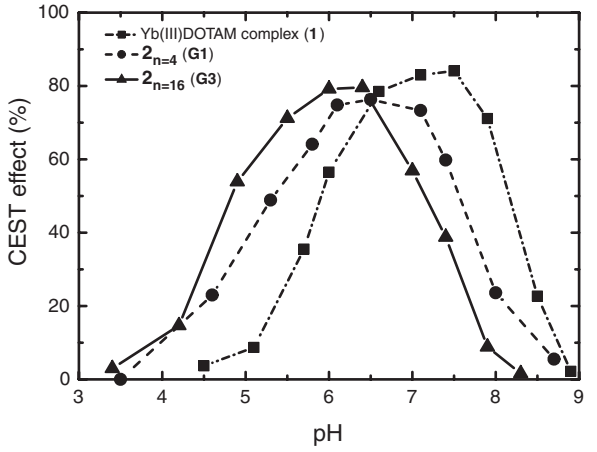

Figure 8. The CEST effect of aqueous solutions (6 mM MOPS) of complexes **1** [c(Yb) = 30 mM], $\mathbf{2}_{n=4}$ (G1) [$c(\mathbf{2}_{n=4})$ = 7.4 mM; c(Yb) = 30 mM] and $\mathbf{2}_{n=16}$ (G3) [$c(\mathbf{2}_{n=16})$ = 1.9 mM; c(Yb) = 30 mM] as a function of pH at 7 T and 310 K. CEST effects were determined using continuous-wave irradiation (2 s duration; 22 μT amplitude) for selective presaturation at −4050 Hz and at +4050 Hz (relative to the water frequency).

Therefore the exchange rate and thus the CEST effect are expected to show a strong pH dependence, with a minimum value at a pH of about 3 (42). At pH values above 7.5, the increase of the CEST effect leveled off and turned into a decrease. This suggests that above pH 7.5 the fast proton exchange regime ($\tau_M \Delta\omega < 1$) is entered. The maximum CEST effect for **1** was observed at pH 7.5 (84% at a concentration of 30 mM).

For the Yb(III)DOTAM-terminated poly(propylene imine) dendrimers a similar pH dependence of the CEST effect was found. However, the maximum CEST effect shifted towards lower pH values for the dendritic PARACEST agents relative to complex **1**. Compound $\mathbf{2}_{n=4}$ (**G1**) showed a maximum CEST effect at pH 6.5. The maximum CEST effect of $\mathbf{2}_{n=16}$ (**G3**) was observed at pH 6.2, a full pH unit lower compared with **1**. Thus, at the same pH of the bulk solution, exchange rates appear to be larger for the dendritic CAs, possibly because the multiple tertiary amine groups of the dendritic core create a micro-environment that is more basic than the bulk (37). This has great potential for practical use, since different pH profiles are needed for different clinical applications of CEST. For instance, CEST-MRI pH mapping in the clinically relevant range between pH 6.5 (the expected pH of tumorous or infarcted tissue) and 7.5 (healthy tissue) (9,43), using the classic ratiometric method for concentration elimination, requires two different exchangeable-proton pools. The first proton pool should show a maximum CEST effect at a pH of ideally slightly lower than 6.5, as found for the third-generation Yb(III)DOTAM-terminated poly(propylene imine) dendrimers. The maximum CEST effect of the second pool should appear at a pH of ideally slightly higher than 7.5, as found for Yb(III)DOTAM. If only a single pH-dependent CEST CA would be used, this should show a maximum CEST effect at pH 6.5, to obtain the strongest signal for tumorous or infarcted tissue. In this case, the dependence of the CEST effect on the local temperature and concentration, would require an independent determination of these parameters (21,44,45). The dendritic framework is highly suitable in this respect, since it allows to couple both, pH-responsive and pH-unresponsive CEST probes to a single dendrimer molecule.

Detection limits of CEST CAs

The CEST effect of complex **1** as a function of the concentration (pH 7.4, 7 T and 310 K) is shown in Fig. 9a. In all experiments for the determination of the concentration dependence of the CEST effect, the pH

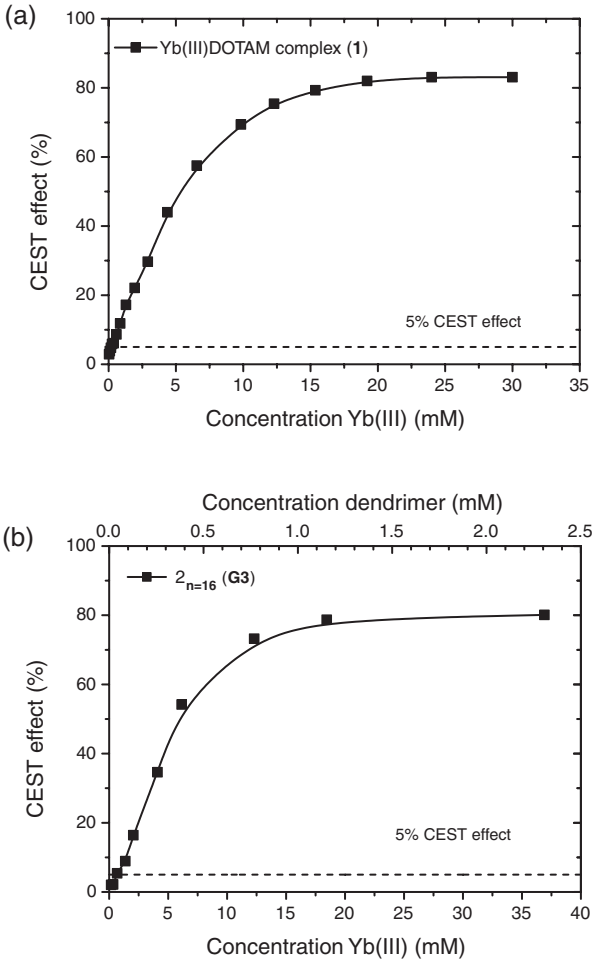

Figure 9. The CEST effect of aqueous solutions (6 mM MOPS) of complexes **1** (a, pH 7.4) and $\mathbf{2}_{n=16}$ (G3) (b, pH 6.3) at 7 T and 310 K. The solid lines were added to guide the eye. The concentration of the dendrimer was calculated by dividing the Yb concentration through the theoretical number of end-groups per dendrimer molecule. CEST effects were determined using continuous-wave irradiation (2 s duration; 22 μT amplitude) for selective presaturation at −4050 Hz and at +4050 Hz (relative to the water frequency).

DOI: 10.1002/cmmi

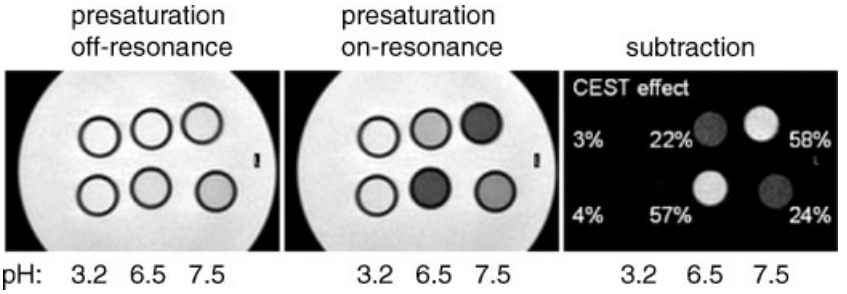

Figure 10. Proton-density weighted turbo spin echo images of aqueous solutions containing **1** (13 mM, top row) and $\mathbf{2}_{n=16}$ (G3) (0.8 mM, bottom row) at a pH of 3.2, 6.5 and 7.5, respectively (3 T and 298 K), with presaturation at −2000 Hz (on resonance) and +2000 Hz (off resonance) relative to the water resonance frequency. The CEST effects are indicated in the subtraction image (right).

was chosen slightly lower than the pH, at which the maximum CEST effect was observed, as a compromise between obtaining the maximum CEST effect and avoiding the fast-exchange regime. Figure 9b shows the CEST effect of $\mathbf{2}_{n=16}$ (**G3**) as a function of the concentration (pH 6.3 and 310 K). From the concentration profiles in Fig. 9 the CEST detection limits (concentration at which the CEST effect is 5%) were determined to be 0.3 ± 0.1 mM for **1** and 0.02 ± 0.01 mM for $\mathbf{2}_{n=16}$ (**G3**). Moreover, the lowest detectable concentration of $\mathbf{2}_{n=4}$ (**G1**) is a factor of 4 lower compared with complex **1** (see supplementary information, Figure S3). Hence, as expected based on the different numbers of exchangeable amide protons, the lowest detectable concentrations of the first- and third- generation dendritic PARACEST agents are approximately a factor of 4 and 16 lower compared with that of complex **1**. A further decrease of the molar detection limit seems feasible by using higher generations of the poly(propylene imine) dendrimer. On the other hand, the lowest detectable concentration of $\mathbf{2}_{n=16}$ (**G3**) is one order of magnitude higher than that of an earlier reported polymeric PARACEST agent that comprises a supramolecular adduct between a positively charged diamagnetic molecule containing the exchangeable-proton pool and a negatively charged paramagnetic shift reagent (28). Although the supramolecular approach offers a higher sensitivity, the increased molecular size may alter the pharmacokinetic properties of the CA.

CEST MR imaging at 3 T

Figure 10 shows the CEST image acquired on a Philips 3 T human MRI scanner of a horizontal slice through a phantom containing six vials of 10 mm diameter. The vials were filled with solutions of 13 mM complex **1** or 0.8 mM of $\mathbf{2}_{n=16}$ (**G3**) at three different pH values at 298 K. (A temperature of 298 K instead of 310 K was chosen for the CEST measurements at 3 T, since it was not possible to maintain the phantom at 310 K in the clinical MRI scanner.) The CEST effects observed at 3 T were lower than those measured at 7 T. The difference can be explained by the shorter T_1 due to the lower field strength and temperature, the lower exchange rate due to the lower temperature, and the smaller frequency difference between the water and the exchangeable-proton signals at lower magnetic field strengths, which causes more direct saturation of the bulk water at an identical saturation power. As expected based on the data obtained at 7 T, for compound **1** the highest CEST effect was measured at pH 7.5, whereas for $\mathbf{2}_{n=16}$ (**G3**) the highest CEST effect was observed at pH 6.5. Additional considerations for CEST imaging on a clinical scanner involve both specific absorption rate (SAR) limits and hardware performance. The 3 T CEST experiments were performed within the limits of the SAR model that is implemented on the scanner. Therefore, the repetition time (*TR*) was chosen to keep the overall power deposition within these limits. However, the model as implemented does not account properly for the high peak deposition during the CEST saturation, spanning 1.6 s. These specific SAR aspects are part of our current research program toward *in vivo* applications of these new CEST CAs.

CONCLUSIONS

A convenient methodology for the synthesis of Yb(III)-DOTAM-terminated poly(propylene imine) dendrimers has been developed and the applicability of these dendritic PARACEST agents has been evaluated *in vitro*. As expected based on the different numbers of exchangeable amide protons, the lowest detectable concentration of the third-generation dendritic PARACEST agent is lower by a factor of about 16 compared with mononuclear reference complex **1**. Upon going from the mononuclear reference complex **1** to the third-generation dendritic PARACEST agent, a shift of the maximum CEST effect from pH 7.5 to 6.5 was observed. This shows that the

DOI: 10.1002/cmmi

responsive pH region of the dendritic CEST agents can be fine-tuned by varying the dendritic framework.

EXPERIMENTAL

General procedures

Unless stated otherwise, all reagents and chemicals were obtained from commercial sources and used without further purification. Dichloromethane (DCM) was dried by distillation from P_2O_5. Water was demineralized prior to use. 2-(*1H*-Benzotriazole-1-yl)-1,1,3,3-tetramethyluronium hexafluorophosphate (HBTU) was purchased from Iris Biotech GmbH (Germany). The first and third generations of amine-terminated poly(propylene imine) dendrimers [DAB-*dendr*-$(NH_2)_n$, $n = 4$ and 16] were kindly provided by SyMO-Chem (Eindhoven, the Netherlands) (46). Cyclen was obtained from ABCR GmbH (Karlsruhe, Germany). Mono *N*-Cbz-protected-1,5-pentyldiamine was prepared according to a literature procedure (47). Molecular characterization of the prepared compounds was performed by ^{1}H NMR and ^{13}C NMR spectroscopy using a Varian Mercury Vx 400 MHz or a Varian Gemini 300 MHz spectrometer at 298 K, and by mass spectrometry using a Perceptive Biosystems Voyager DE-PRO MALDI-TOF mass spectrometer or a Finnigan LCQ Decca XP Max ESI mass spectrometer. The pH was measured using a calomel combination pH electrode (3.5 × 183 mm, Sigma Aldrich) with an accuracy of 0.01 at room temperature. No temperature correction was performed.

NMR spectroscopy

NMR samples were prepared by dissolving the appropriate amount of CEST agent in a mixture of H_2O (400 μl) and 100 mM MOPS buffer pH 6.9 (25 μl). The pH values of the solutions were adjusted by adding small aliquots of either 0.1 M NaOH or 0.1 M HCl stock solutions. To enable frequency locking, a coaxial glass capillary insert filled with deuterated tetrachloroethane was used. NMR spectra were recorded on a Bruker Avance NMR spectrometer equipped with an Oxford wide-bore 7 T superconducting magnet. One-dimensional NMR measurements were performed without water suppression. For the one-dimensional NMR spectra, 128 k complex data points were acquired with a dwell time of 200 μs. For ^{1}H NMR spectra in D_2O, the residual HDO signal was suppressed using standard continuous-wave presaturation (2 s pulse duration) at the HDO resonance frequency. Prior to Fourier transformation, the data were apodized with an exponential filter (line broadening = 5 Hz). All spectra were calibrated relative to the H_2O or HDO frequency. CEST spectra were recorded using standard continuous-wave irradiation (2 s pulse duration; 22 μT pulse amplitude) for selective presaturation of the exchangeable-proton resonance. Typically, 121 individual one-dimensional ^{1}H NMR spectra were acquired at different values of the presaturation offset frequency (150 Hz intervals) centered around the water resonance frequency and stored in a single two-dimensional NMR data set. To reconstruct the CEST spectrum, the water signal of each individual spectrum in the two-dimensional data set was integrated and plotted as a function of the presaturation offset frequency. From the resulting spectrum the CEST effect was determined using eqn (1).

MR imaging

CEST MR images were acquired on a Philips Achieva 3 T whole-body MRI scanner (Philips Medical Systems, Best, the Netherlands) using a human transmit-receive head coil and a turbo spin-echo pulse sequence (turbo factor 20; $TE = 8$ ms; $TR = 25.3$ s, slice thickness = 6 mm; FOV = 23 × 23 cm^2; matrix size = 256 × 256 voxels). A continuous wave irradiation pulse (1600 ms), implemented as a continuous train of 32 × 50 ms, 10.5 μT rectangular RF pulses (without delay), was used for selective saturation. The total pulse length and shape were determined by technical and SAR limits of the clinical MRI scanner. The measuring time per image was 5.8 min. The carrier frequency of the saturation pulses was either −2 kHz (for the CEST-attenuated image M_S) or +2 kHz (for the reference image M_0) relative to the water resonance frequency. With these experimental settings, FDA limits on specific absorption rates (SAR) for MR imaging of the human head were not exceeded (48).

Synthesis

Yb(III)DOTAM-based complex 1. A solution of $YbCl_3 \cdot 6H_2O$ (35.6 mg, 91.8 μmol) in H_2O (0.5 ml) was added dropwise to a solution of **9** (59.9 mg, 96.6 μmol) in H_2O (10 ml). The solution was stirred at 60°C for 4 h, while maintaining the pH at 7–8 by adding small aliquots of NH_4OH (aq). Lyophilization yielded complex **1**. This product was used in NMR studies without further purification. ESI-MS *m/z* 791.7 ($[M-2H]^+$).

Yb(III)DOTAM-terminated poly(propylene imine) dendrimers (2_n). $\mathbf{2}_{n=4}$ (**G1**). DOTAM-terminated poly (propylene imine) dendrimer $\mathbf{8}_{n=4}$ (74.2 mg, 40.1 μmol) was dissolved in H_2O (7 ml) and the pH of the solution was adjusted to 7 with NH_4OH (aq). The solution was vigorously stirred at 60°C and $YbCl_3 \cdot 6H_2O$ (58.9 mg, 152 μmol) dissolved in H_2O (0.5 ml) was added. The pH was maintained with NH_4OH (*aq*) at 7–8. The solution was stirred for 4 h at RT. Lyophilization yielded $\mathbf{2}_{n=4}$.

DOI: 10.1002/cmmi

$2_{n=16}$ (G3). **$8_{n=16}$** (72.8 mg, 9.3 μmol) was dissolved in H_2O (10 ml). The pH of the solution was adjusted to 7 with 0.1 M NH_4OH (aq). The solution was vigorously stirred at 60°C and a mixture of $YbCl_3{\cdot}6H_2O$ (54.6 mg, 141 μmol) in H_2O (0.5 ml) was added. The pH was maintained at 7–8 and the solution was stirred for 4 h. Lyophilization yielded **$2_{n=16}$**.

1,4,7-Tris(tert-butyloxycarbonyl)-1,4,7,10-tetraazacyclododecane (3). This compound was prepared according to a procedure described by Kimura *et al* (49).

1-(Benzyloxycarbonylmethyl)-4,7,10-tris(tert-butyloxycarbonyl)-1,4,7,10-tetraazacyclododecane (4). Compound **3** (15.2 g, 32.2 mmol) was dissolved in acetonitrile (20 ml). Subsequently, a solution of *N*,*N*-diisopropylethylamine (19 ml, 0.11 mol) and benzyl bromoacetate (7.90 g, 34.5 mmol) in acetonitrile (10 ml) was added. The solution was stirred overnight at 60°C in an argon atmosphere. The obtained mixture was concentrated under reduced pressure and dissolved in DCM. The solution was washed with 1 M NaOH and dried over Na_2SO_4. After filtration, the solution was concentrated under reduced pressure and co-evaporated with toluene (2 × 50 ml). The crude product was purified by column chromatography over silica gel eluting with hexane/EtOAc (1:1). Compound **4** (17.9 g, 28.9 mmol) was obtained in 90% yield. ^{1}H NMR ($CDCl_3$): δ 7.4 (m, 5H, Ph-H), 5.2 (s, 2H, CH_2Ph), 3.6 [s, 2H, $CH_2C(O)$], 3.6–3.2 (m, 12H, CH_2N), 2.9 (b, 4H, CH_2N), 1.5 (s, 9H, CH_3), 1.4 (s, 18H, CH_3) ppm. ^{13}C NMR ($CDCl_3$): δ 170.3 (C=O ester), 156–155 (multiple signals C=O urethanes), 135.5 and 128.6–128.2 (aromatic carbons), 79.5–79.2 (multiple signals CCH_3), 66.2 (CH_2O), 55.0, 53.5, 51.2, 49.9 and 47.4–46.9 (CH_2N), 28.6 (CH_3), 28.4 (CH_3) ppm. ESI-MS *m/z* 621.3 ($[M+H]^+$).

1-(Benzyloxycarbonylmethyl)-4,7,10-tris(carbamoylmethyl)-1,4,7,10-tetraaza-cyclododecane (6). To an ice-cooled solution of **4** (6.22 g, 10.0 mmol) in DCM (60 ml) was added trifluoroacetic acid (TFA, 60 ml). The solution was stirred for 3 h in a nitrogen atmosphere. The solution was concentrated under reduced pressure at room temperature and TFA (40 ml) was added. The solution was stirred for 2 h at room temperature, concentrated *in vacuo*, and co-evaporated with toluene (twice) to yield the TFA salt of **5**. This compound was dissolved in a mixture of DMF (45 ml) and *N*,*N*-diisopropylethylamine (30 ml, 0.17 mol). Subsequently, 2-bromoacetamide (4.7 g, 34 mmol) was added and the mixture was stirred at 50°C for 2 days. The mixture was poured into Et_2O (600 ml) and the brownish precipitate was isolated by filtration. The solid was washed with 25% NH_3 (aq) (4 × 25 ml) and H_2O (30 ml). The product was dried *in vacuo* at 40°C to give a white solid (4.19 g, 8.52 mmol) in a yield of 85%. ^{1}H NMR (DMSO-d_6 with a drop of D_2O): δ 7.4 (m, 5H, Ph-H), 5.1 (s, 2H, Ph-CH_2), 3.5 (s, 2H, $CH_2C(O)O$), 3.0 (s, 2H, $CH_2C(O)NH_2$), 2.9 (s, 4H, $CH_2C(O)NH_2$), 2.7 (b, 4H, CH_2N), 2.5 (b, 12H, CH_2N and NH_2) ppm. ^{13}C NMR (DMSO-d_6 with a drop of D_2O): δ 173.4 and 173.1 (C=O amides), 171.0 (C=O ester), 136.5 and 129–128 (aromatic carbons), 65.5 (CH_2O), 58.1, 54.9, 53.4, 53.1 and 51.9 (CH_2N) ppm. MALDI-TOF-MS: 492 ($[M+H]^+$), 514 ($[M+Na]^+$), 530 ($[M+K]^+$).

4,7,10-Tris(carbamoylmethyl)-1,4,7,10-tetraazacyclododecane-1-yl-acetic acid (7). The hydrogenation of **6** (0.900 g, 1.83 mmol) in H_2O (60 ml) was performed in a Parr hydrogenation apparatus at 70 psi hydrogen pressure overnight using 10% Pd/C (41 mg) as the catalyst. The mixture was filtered over Celite and the filtrate was lyophilized. The obtained white hygroscopic powder (0.698 g, 1.74 mmol, 95%) was dried over P_2O_5. ^{1}H NMR (D_2O): δ 3.7 (s, 2H, CH_2COOH), 3.3 (b, 4H, CH_2N), 3.2 (b, 4H, CH_2N), 3.0 (s, 2H, $CH_2C(O)NH_2$), 2.9 (b, 4H, CH_2N), 2.6 (b, 8H, CH_2N) ppm. ^{13}C NMR (D_2O): δ 173.6 and 176.2 (C=O amides), 170.5 (C=O), 57.0, 56.7, 56.5, 53.1, 51.0, 50.6 and 47.8 (CH_2N) ppm. MALDI-TOF-MS: 402 ($[M+H]^+$), 424 ($[M+Na]^+$), 440 ($[M+K]^+$).

DOTAM-terminated poly(propylene imine) dendrimers (8_n = 4,16). **$8_{n=16}$**. *N*,*N*-Diisopropylethylamine (0.25 ml, 1.4 mmol) and HBTU (0.164 g, 0.43 mmol) were mixed in DMF (1 ml). Compound **7** (0.172 g, 0.43 mmol) in dry DMF (1 ml) was added and the mixture was stirred for 5 min in a nitrogen atmosphere. Subsequently, DAB-*dendr*-$(NH_2)_{n=16}$ (41 mg, 24 μmol) in dry DMF (1 ml) was added and the solution was stirred overnight in a nitrogen atmosphere. The product was precipitated in Et_2O (40 ml), filtered, washed with Et_2O and dried. The precipitate was dissolved in water, triethylamine was added and extensively dialyzed using a membrane with a MWCO of 1 kDa. Freeze-drying afforded **$8_{n=16}$** as a fluffy white powder (0.18 g). ^{1}H NMR (D_2O): δ 3.2–3.0, 2.7–2.5, 2.5–2.3, 1.7–1.5 ppm. ^{13}C NMR (D_2O): δ 177, 173, 58–56, 53–50, 39, 37, 25, 21 ppm. MALDI-TOF-MS: 7823 ($[M+H]^+$); ESI-MS *m/z* 7823 ($[M+H]^+$).

$8_{n=4}$. A similar synthetic procedure as used for **$8_{n=16}$** was applied for the synthesis of **$8_{n=4}$**, using the first generation of the amine-terminated poly(propylene imine) dendrimer. ^{1}H NMR (D_2O): δ 3.1, 3.0, 2.6, 2.3, 1.6, 1.5, 1.3 ppm. ^{13}C NMR: δ 177.5, 173.8, 58.6–57.3, 53.4–52.7, 50.8, 39.3, 37.6, 25.6, 23.8 ppm. MALDI-TOF-MS: 1851 ($[M+H]^+$), 1873 ($[M+Na]^+$) and 1889 ($[M+K]^+$).

1-(5-benzyloxyamidopentyl)carbamoylmethyl-4,7,10-tris(carbamoylmethyl)-1,4,7,10-tetraazacyclododecane (9). *N*,*N*-Diisopropylethylamine (0.36 ml, 2.1 mmol) and HBTU (0.312 g, 0.82 mmol) were mixed in

DOI: 10.1002/cmmi

DMF (2 ml). Compound **7** (0.300 g, 0.748 mmol) in dry DMF (2 ml) was added and the mixture was stirred for 5 min in a nitrogen atmosphere. Subsequently, mono *N*-Cbz-protected-1,5-pentamethylenediamine (0.167 g, 0.712 mmol) in dry DMF (2 ml) was added and the obtained solution was stirred overnight under an atmosphere of nitrogen. The product was precipitated in Et_2O (40 ml), filtered, washed with Et_2O and dried *in vacuo*. ^{1}H NMR (CD_3OD): δ 7.4 (m, 5H), 5.1 (s, 2H), 3.3 (m, 2H), 3.1 (m, 10H), 2.6 (m, 16H), 1.6 (m, 4H), 1.4 (m, 2H) ppm. MALDI-TOF-MS: 620.6 ($[M+H]^+$), 642.6 ($[M+Na]^+$), 658.6 ($[M+K]^+$).

Acknowledgements

This work was financially supported by the BSIK-program Molecular Imaging of Ischemic Heart Disease (project number BSIK03033).

REFERENCES

1. Merbach AE, Tóth E. *The chemistry of contrast agents in medical magnetic resonance imaging*. John Wiley & Sons: New York, 2001.
2. Caravan P, Ellison JJ, McMurry TJ, Lauffer RB. Gadolinium(III) chelates as MRI contrast agents: structure, dynamics, and applications. *Chem. Rev.* 1999; **99**: 2293–2352.
3. Aime S, Botta M, Crich SG, Giovenzana G, Palmisano G, Sisti M. A macromolecular Gd(III) complex as pH-responsive relaxometric probe for MRI applications. *Chem. Commun.* 1999; 1577–1578.
4. Zhang SR, Wu KC, Sherry AD. Gd3+ complexes with slowly exchanging bound-water molecules may offer advantages in the design of responsive MR agents. *Invest. Radiol.* 2001; **36**: 82–86.
5. Hovland R, Glogard C, Aasen AJ, Klaveness J. Gadolinium DO3A derivatives mimicking phospholipids; preparation and in vitro evaluation as pH responsive MRI contrast agents. *Perkin Trans.* 2001; **2**: 929–933.
6. Raghunand N, Zhang SR, Sherry AD, Gillies RJ. In vivo magnetic resonance imaging of tissue pH using a novel pH-sensitive contrast agent, GdDOTA-4AmP. *Acad. Radiol.* 2002; **9**: S481–S483.
7. Laus S, Sour A, Ruloff R, Toth E, Merbach AE. Rotational dynamics account for pH-dependent relaxivities of PAMAM dendrimeric, Gd-based potential MRI contrast agents. *Chem. Eur. J.* 2005; **11**: 3064–3076.
8. Zhang SR, Wu KC, Sherry AD. A novel pH-sensitive MRI contrast agent. *Angew. Chem. Int. Ed.* 1999; **38**: 3192–3194.
9. Vaupel P, Kallinowski F, Okunieff P. Blood-Flow, Oxygen and Nutrient Supply, and Metabolic Microenvironment of Human-Tumors - A Review. *Cancer Res.* 1989; **49**: 6449–6465.
10. Aime S, Carrera C, Castelli DD, Crich SG, Terreno E. Tunable imaging of cells labeled with MRI-PARACEST agents. *Angew. Chem. Int. Ed.* 2005; **44**: 1813–1815.
11. Weissleder R, Mahmood U. Molecular imaging. *Radiology* 2001; **219**: 316–333.
12. Lee AS, Weissleder R, Brady TJ, Wittenberg J. Lymph-Nodes - Microstructural Anatomy at MR Imaging. *Radiology* 1991; **178**: 519–522.
13. Anzai Y, Piccoli CW, Outwater EK, Stanford W, Bluemke DA, Nurenberg P, Saini S, Maravilla KR, Feldman DE, Schmiedl UP, Brunberg JA, Francis IR, Harms SE, Som PM, Tempany CM. Evaluation of neck and body metastases to nodes with ferumoxtran 10-enhanced MR imaging: Phase III safety and efficacy study. *Radiology* 2003; **228**: 777–788.
14. Torabi M, Aquino SL, Harisinghani MG. Current concepts in lymph node imaging. *J. Nucl. Med.* 2004; **45**: 1509–1518.
15. Aime S, Delli Castelli D, Terreno E. Novel pH-reporter MRI contrast agents. *Angew. Chem. Int. Ed.* 2002; **41**: 4334–4336.
16. Ward KM, Aletras AH, Balaban RS. A new class of contrast agents for MRI based on proton chemical exchange dependent saturation transfer (CEST). *J. Magn. Reson.* 2000; **143**: 79–87.
17. Forsen S, Hoffman RA. Study of Moderately Rapid Chemical Exchange Reactions by Means of Nuclear Magnetic Double Resonance. *J. Chem. Phys.* 1963; **39**: 2892–2901.
18. Forsen S, Hoffman RA. Exchange Rates by Nuclear Magnetic Multiple Resonance .3. Exchange Reactions in Systems with Several Non-Equivalent Sites. *J. Chem. Phys.* 1964; **40**: 1189–1196.
19. Ward KM, Balaban RS. Determination of pH using water protons and chemical exchange dependent saturation transfer (CEST). *Magn. Reson. Med.* 2000; **44**: 799–802.
20. Zhang SR, Michaudet L, Burgess S, Sherry AD. The amide protons of an ytterbium(III) dota tetraamide complex act as efficient antennae for transfer of magnetization to bulk water. *Angew. Chem. Int. Ed.* 2002; **41**: 1919–1921.
21. Aime S, Barge A, Castelli DD, Fedeli F, Mortillaro A, Nielsen FU, Terreno E. Paramagnetic lanthanide(III) complexes as pH-sensitive chemical exchange saturation transfer (CEST) contrast agents for MRI applications. *Magn. Reson. Med.* 2002; **47**: 639–648.
22. Zhang SR, Winter P, Wu KC, Sherry AD. A novel europium(III)-based MRI contrast agent. *J. Am. Chem. Soc.* 2001; **123**: 1517–1518.
23. Zhang SR, Merritt M, Woessner DE, Lenkinski RE, Sherry AD. PARACEST agents: Modulating MRI contrast via water proton exchange. *Acc. Chem. Res.* 2003; **36**: 783–790.
24. Ahrens ET, Rothbacher U, Jacobs RE, Fraser SE. A model for MRI contrast enhancement using T_1 agents. *Proc. Natl. Acad. Sci. U.S.A.* 1998; **95**: 8443–8448.
25. Goffeney N, Bulte JWM, Duyn J, Bryant LH, van Zijl PCM. Sensitive NMR detection of cationic-polymer-based gene delivery systems using saturation transfer via proton exchange. *J. Am. Chem. Soc.* 2001; **123**: 8628–8629.
26. Sun PZ, Zhou JY, Sun WY, Huang J, van Zijl PCM. Suppression of lipid artifacts in amide proton transfer imaging. *Magn. Reson. Med.* 2005; **54**: 222–225.
27. Zhou JY, van Zijl PCM. Chemical exchange saturation transfer imaging and spectroscopy. *Progr. Nucl. Magn. Reson. Spectr.* 2006; **48**: 109–136.
28. Aime S, Delli Castelli D, Terreno E. Supramolecular adducts between poly-L-arginine and [Tm(III)dotp]: A route to sensitivity-enhanced magnetic resonance imaging-chemical exchange saturation transfer agents. *Angew. Chem. Int. Ed.* 2003; **42**: 4527–4529.
29. Zhang S, Michadet L, Sherry AD. PARACEST agents based upon DOTA-like conjugates with poly-L-lysine. *Proc. Int. Magn. Reson. Med.* 2005; **13**: 2708.
30. Terreno E, Cabella C, Carrera C, Castelli DD, Mazzon R, Rollet S, Stancanello J, Visigalli M, Aime S. From spherical to osmotically shrunken paramagnetic liposomes: An improved generation of LIPOCEST MRI agents with highly shifted water protons. *Angew. Chem. Int. Ed.* 2007; **46**: 966–9968.
31. Aime S, Castelli DD, Terreno E. Highly sensitive MRI chemical exchange saturation transfer agents using liposomes. *Angew. Chem. Int. Ed.* 2005; **44**: 5513–5515.
32. Wiener EC, Brechbiel MW, Brothers H, Magin RL, Gansow OA, Tomalia DA, Lauterbur PC. Dendrimer-based metal chelates: a new class of magnetic resonance imaging contrast agents. *Magn. Reson. Med.* 1994; **31**: 1–8.
33. Kobayashi H, Kawamoto S, Jo S-K, Bryant HL Jr, Brechbiel MW, Star RA, Macromolecular MRI contrast agents with small dendrimers: pharmacokinetic differences between sizes and cores. *Bioconjug. Chem.* 2003; **14**: 388–394.
34. Langereis S, de Lussanet QG, van Genderen MHP, Backes WH, Meijer EW. Multivalent contrast agents based on gadolinium-diethylenetriaminepentaacetic acid-terminated poly(propylene imine) dendrimers for magnetic resonance imaging. *Macromolecules* 2004; **37**: 3084–3091.
35. Langereis S, de Lussanet QG, van Genderen MHP, Meijer EW, Beets-Tan RGH, Griffioen AW, van Engelshoven JMA, Backes WH. Evaluation of Gd(III)DTPA-terminated poly(propylene imine) dendrimers as contrast agents for MR imaging. *NMR Biomed.* 2006; **19**: 133–141.

36. de Lussanet QG, Langereis S, Beets-Tan RGH, van Genderen MHP, Griffioen AW, van Engelshoven JMA, Backes WH. Dynamic contrast-enhanced MR imaging kinetic parameters and molecular weight of dendritic contrast agents in tumor angiogenesis in mice. *Radiology* 2005; **235**: 65–72.
37. Koper GJM, van Genderen MHP, Elissen-Roman C, Baars MWPL, Meijer EW, Borkovec M. Protonation Mechanism of Poly(propylene imine) Dendrimers and Some Associated Oligo Amines. *J. Am. Chem. Soc.* 1997; **119**: 6512–6521.
38. McMahon MT, Gilad AA, Zhou J, Sun PZ, Bulte JWM, van Zijl PCM. Quantifying exchange rates in chemical exchange saturation transfer agents using the saturation time and saturation power dependencies of the magnetization transfer effects on the magnetic resonance imaging signal (QUEST and QUESP): pH calibration for poly-L-lysine and a starburst dendrimer. *Magn. Reson. Med.* 2006; **55**: 836–847.
39. Liepinsh E, Otting G. Proton exchange rates from amino acid side chains - Implications for image contrast. *Magn. Reson. Med.* 1996; **35**: 30–42.
40. Englander SW, Downer NW, Teitelbaum H. Hydrogen-Exchange. *Annu. Rev. Biochem.* 1972; **41**: 903–924.
41. Constable EC. *Metals and Ligand Reactivity: An Introduction to the Organic Chemistry of Metal Complexes*. VCH Weinheim: 1995.
42. Connelly GP, Bai YW, Jeng MF, Englander SW. Isotope Effects in Peptide Group Hydrogen-Exchange. *Proteins: Structure Funct. Genet.* 1993; **17**: 87–92.
43. Gillies RJ, Raghunand N, Garcia-Martin ML, Gatenby RA. pH imaging. *IEEE Engineering in Medicine and Biology Magazine* 2004; **23**: 57–64.
44. Terreno E, Castelli DD, Cravotto G, Milone L, Aime S. Ln(III)-DOTAMGly complexes: A versatile series to assess the determinants of the efficacy of paramagnetic chemical exchange saturation transfer agents for magnetic resonance imaging applications. *Invest. Radiol.* 2004; **39**: 235–243.
45. Garcia-Martin ML, Martinez GV, Raghunand N, Sherry AD, Zhang SR, Gillies RJ. High resolution pH(e) imaging of rat glioma using pH-dependent relaxivity. *Magn. Reson. Med.* 2006; **55**: 309–315.
46. Maliakal AJ, Turro NJ, Bosman AW, Cornel J, Meijer EW. Relaxivity Studies on Dinitroxide and Polynitroxyl Functionalized Dendrimers: Effect of Electron Exchange and Structure on Paramagnetic Relaxation Enhancement. *J. Phys. Chem. A*. 2003; **107**: 8467–8475.
47. Pittelkow M, Lewinsky R, Christensen JB. Selective synthesis of carbamate protected polyamines using alkyl phenyl carbonates. *Synthesis* 2002; 2195–2202.
48. Details concerning the SAR limits can be found on the following FDA website http://www.fda.gov/cdrh/ode/primerf6.html (last accessed in July 2007).
49. Kimura E, Aoki S, Koike T, Shiro M. A Tris(zinc-1,4,7,10-tetraazacyclododecane) Complex as a New Receptor for Phosphate Dianions in Aqueous Solution. *J. Am. Chem. Soc.* 1997; **119**: 3068–3076.
50. Aoki S, Kawatani H, Goto T, Kimura E, Shiro M. A Double-Functionalized Cyclen with Carbamoyl and Dansyl Groups (Cyclen = 1,4,7,10-Tetraazacyclododecane): A Selective Fluorescent Probe for Y^{3+} and La^{3+}. *J. Am. Chem. Soc.* 2001; **123**: 1123–1132.

DOI: 10.1002/cmmi